)

MHD INSTABILITIES IN SHEAR FLOWS OF ANISOTROPIC COSMIC PLASMAS. I. FIRE HOSE MODES

N. S. Dzhalilov [a*], ***J. H. Samadov*** [a]

[a] *N.Tusi Shamakhy Astrophysical Observatory of Azerbaijan National Academy of Sciences, Shamakhy, Azerbaijan*

The stability of the anisotropic collisionless plasma layer to small disturbances in the MHD description is studied based on moment equations obtained from the Vlasov kinetic equation taking into account the heat flow along the spatially shearing flow. To find the complex spectral parameter that determines the growth rate of instability, on the base of the obtained wave equation, the boundary value problem is solved using WKB approximation for the case of a smooth hyperbolic velocity profile. A general integral dispersion equation, based on these solutions is obtained. This equation describes all types of body and interface instabilities in the presence of heat flow along the magnetic field, well studied for infinite stationary and homogeneous anisotropic plasma. It is shown that reducing the layer width greatly enhances the mirror instability, and strongly suppresses the oblique fire-hose instability. We limited ourselves here to study how the spatial gradient of the plasma flow affects the properties of an aperiodical oblique fire-hose instability in a limited layer. It was found that the spatial gradient in flow velocity greatly enhances this instability. With a narrowing of the shearing layer width and an increasing of the velocity gradient, the body hose modes transform into surface Kelvin-Helmholtz modes existing on the interface between the two parts of the flow with the different velocities.

Keywords: Solar wind – anisotropic plasma instability – MHD shearing flows

1. INTRODUCTION

In collisionless plasmas, the mechanism of dissipation of the energy contained in macroscopic scales is still a matter of considerable debate (Cranmer et al. 2015)

)https://doi.org/10.59849/2078-4163.2024.1.40

* E-mail: dnamig@gmail.com

[9]. The primary mechanism is considered to be the turbulent transfer of energy from macroscales to microscales (to scales such as the ion gyro-radius and ion inertial length), resulting in the conversion of energy into heat through kinetic processes (e.g. Marsch 2006) [42]. The transition between the scales occurs in a cascade (e.g.Loureiro & Boldyrey 2017) [37], and on kinetic scales processes such as wave-particle resonances (e.g. Gary et al. 2016) [20] and various plasma processes in coherent structures come into play(e.g. Chasapis et al. 2017; Jain et al. 2021) [10, 33]. The turbulent cascade mechanism is often used to explain plasma heating under cosmic conditions, such as coronal heating and solar wind generation(e.g. Kiyani et al. 2015; Verdini et al. 2019) [33, 34]. Turbulence scales can be conditionally divided into cascade stages: energy-containing macroscales, inertial acceleration scales, and resonant dissipative scales. We are interested in the onset of turbulence formation (instability of the ground state of the plasma) at macroscopic scales, which contain the bulk of the energy. In the case of low-collision plasmas, the theory is complicated by the fact that rarefied hot plasmas in the presence of a magnetic field become highly anisotropic relative to the direction of the external magnetic field, such as in the solar wind. Pressure anisotropy can cause additional instabilities, both in micro and macro scales (e.g. Vedenov & Sagdeev 1958) [56], which tend to bring the plasma into a thermodynamic equilibrium state. Micro-instabilities play an important role for macroscale energy redistribution (e.g.Verscharen et al. 2019) [58]. However, the observed anisotropies, for example, in the solar wind (e.g.Hellinger et al. 2006) [25], are remarkably stable and long-lived (Bale et al. 2009, Matteini et.al 2013) [2, 38] making them difficult to explain.

The main reason for the development of turbulence is plasma instabilities, i.e., instability can be thought of as the onset of turbulence. The generation and growth of instability are driven by free energy contained in the spatial gradient of the physical parameters of the medium or the non-Maxwellian distribution of plasma particles. The most common source of free energy in nature, including in space, is flows with a velocity gradient. Shear flows of fluid or plasma are usually characterized by a flow velocity gradient across the direction of flow. The simplest example is when plasma slips over a more static environment(e.g. Kivelson & Chen 1995) [36]. Examples include interaction regions that arise between fast and slow flows in the solar wind (Bale et al. 2009, Bruno & Carbone 2013) [1, 2], the interface between the solar wind and a planetary magnetosphere (Hasegawa et al. 2004) [23], the surface of coronal mass ejections (CME) (Foullon et al. 2011) [16], and the surfaces of various astrophysical jets(Hamlin & Newman 2013) [29]. Under such conditions, Kelvin-Helmholtz instability (KHI) can be easily excited by free energy flows with a velocity gradient. If fluid or plasma is considered an incompressible medium, then any value of transverse shear (velocity jump) causes

KHI instability (e.g., Chandrasekhar 1961) [6]. The magnetic field is known to stabilize this instability. However, when the shear becomes larger (usually the threshold is determined by the Alfvén speed in the direction of the flow), instability occurs again. KHI can cause some phenomena that are directly observed. For example, under certain magnetic field configurations, solar flux can penetrate the magnetosphere of planets due to the magnetic reconnection effect(e.g. Sisti et al. 2019) [51] transferring momentum, mass, magnetic flux, and energy. (e.g.Delamare M. et al. 2024) [11]. Interestingly, there are possible situations where newly born KHI vortices, before transitioning to a nonlinear regime and decaying, can transfer energy into the magnetic field and, through the reconnection mechanism, heat the plasma of the corona. (Telloni et al 2022) [52].

Many studies are devoted to the theory of KHI development, both in the MHD approximation (e.g.Walker 1981; Faganello et al. 2008) [17, 59] and in the kinetic description (e.g. Pritchett & Coroniti 1984; Henri et al. 2013) [28, 48]. If the plasma is collisionless and the width of the shear layer is comparable to the ion scales (in the solar wind at a distance of 1 AU, proton inertial length = 140 km, proton gyration radius = 160 km), then the kinetic description is preferable, as seen in Earth's magnetopause.(e.g.Faganello & Califano 2017) [18]. Shear flows are studied mainly in two aspects. If the KHI threshold is not yet reached, then the flow is stable to small perturbations, and various types of MHD waves can propagate in such flows. However, stable waves are strongly affected by shear. For example, the phase mixing mechanism can generate small scales in the direction of the flow velocity gradient (e.g., Pucci & Malara 2014) [46], which can transform ordinary Alfvén waves into kinetic Alfvén waves (Hollweg and Kaghashvili 2012) [31], the dissipation of which can become one of the main heating mechanisms in collisionless plasma. The shear can cause interactions and energy transformation between different types of waves (Pucci et al. 2016) [45]. The fluctuations on smaller scales lead to wave dissipation (e.g., Mok & Einaudi 1985; Hollweg 1987; Kaghashvili 2007; Pucci et al. 2014) [31, 35, 39, 46] which may also contribute to the appearance of anisotropy in the distribution function (e.g., Pezzi et al. . 2017) [47]. In the MHD description at such small scales, taking into account Hall effects becomes important (Vàsconez et al. 2015, Maiorano et al. 2020) [41,57]. If the instability threshold is met, then Kelvin-Helmholtz instability (KHI) occurs. This means that vortex mixing of the shear layer is generated, which in a nonlinear stage, turns into turbulence (Blasl et al. 2022;Hasegawa et al. 2020) [3, 30]. When the shear layer width is on the order of the ionic inertial scale, dispersion effects can strongly modify the KHI. (Chac'on et al. 2003) [5].

In the kinetic description, both for wave propagation and KHI, the construction of the initial stable state of shear flows is a separate, rather complex task (e.g. Guzzi et al.2021) [21]. For the MHD description, this difficulty does not

exist. Therefore, the averaged fluid description of a collisionless plasma, despite its disadvantages (the inability to describe in detail important kinetic effects such as resonant interactions of particles and waves, Landau damping, and others), also has advantages for the case of large-scale and low-frequency phenomena. For example, in the (Wang & Hau 2003) [60] it has been shown that the basic properties of fire hose instabilities (incompressible parallel and compressible inclined) obtained from the kinetic theory are not lost in the fluid approach. The introduction of sufficient viscosity and resistivity into the MHD model also leads to results consistent with the kinetic description for the nonlinear decay stage of the process under consideration.

In a homogeneous anisotropic plasma, classical MHD (shear) Alfvén waves become unstable if the condition $p_{\parallel} > p_{\perp} + B^2/4\pi$ or $\beta_{\parallel} - \beta_{\perp} > 2$ (hose instability) is met. These incompressible modes have the maximum instability growth rate when is propagating in parallel. The second type of hose mode is compressible and has maximum instability when is propagating obliquely (Hellinger & Matsumoto 2000) [26]. This instability has a higher growth rate than the classic hose modes.

In another limit of pressure anisotropy $p_{\parallel} < p_{\perp}$another type of plasma instability arises - obliquely mirror instability. In this limit, kinetic resonance ion cyclotron instabilities are also possible, which do not arise in the MHD description. However, for mirror modes, the instability threshold in the MHD description, taking into account heat flow, exactly coincides with the low-frequency kinetic results, $\beta_{\parallel} < \beta_{\perp}^2/(1+\beta_{\perp})$. Our results (Dzhalilov et al. 2011) [14] are identical to the one based on the linear Vlasov theory (Hau and Sonnerup.1993) [24]. Note that the CGL MHD model (Chew et al. 1956) [4], which admits double-adiabatic laws, does not correspond to the results of the linear Vlasov kinetic theory (e.g., Hasegawa 1975) [22].

In the case of a tangential discontinuity between flows with different velocities, only surface modes arise, including KHI. If the transition from one flow to another has a finite width and a smooth velocity profile (more consistent with real situations), then in this transition layer, in addition to surface modes, body waves are also possible, and they can interact with each other. Issues of the effect of finite width of the transition layer with different velocity profiles in isotropic MHD have been studied, (Ray & Ershkoyich (1983); Miura (1982); Choudhury (1986) ; Uberoi (1986), and in Choudhury & Patel (1985)) [7,8,40,49,54] and the plasma anisotropy were considered within the framework of the CGL MHD model. However, if we consider a layer of anisotropic plasma with a finite width, shear flow, and heat flux, then the following questions arise: 1) If the KHI threshold is not reached, how are MHD waves and associated classical instabilities (fire hose, mirror, and others) modified? 2) If KHI occurs, how is it modified by shear and how do other instabilities and waves change? Our work is devoted to studying

these issues. In this work, we focused on how the second type of fire hose instability (compressible oblique modes) is modified by the shear flow (finite width) of an anisotropic plasma, taking into account heat flux along the magnetic field. Similar questions for classical fire hose modes (incompressible parallel modes) in an infinite medium with a linear velocity gradient were studied using the asymptotic method in (Uchava et al. 2020) [53].

Section 2 presents MHD equations that describe the fluid behavior of a collisionless plasma taking into account the heat flux along the magnetic field. Based on these equations, a general wave equation is obtained for linear disturbances in a plasma layer with shearing in the flow velocity. In section 3, for a smooth hyperbolic flow velocity profile, a boundary value problem is solved based on the WKB approximation. The resulting integral dispersion equation describes the growing rates of all types of instabilities that arise in a shear layer with a finite arbitrary width and with the arbitrary transverse flow velocity gradient. In section 4, the limiting transition to the homogeneous flow, but in a spatially limited plasma layer, is separately studied. Changes in instability grows rates depending on the layer width have been studied. In section 5, oblique compressible aperiodic hose modes in a spatially limited shear layer are studied. Modification of instability depending on the width of the transition layer and the velocity gradient are the main subjects of research. Concluding remarks are provided in section 6.

2. THE BASIC WAVE EQUATIONS IN THE FLUID DESCRIPTION

For the fluid description of a collisionless anisotropic plasma regarding to the direction of the external magnetic field, the 16-moment set of equations may be used which is complete (in comparison of CGL approximation) in the sense that these equations include the evolution of heat fluxes along the magnetic field. [43, 50] For the one component (ion) plasma, these equations are given as follows:

$$\frac{d\rho}{dt} + \rho \operatorname{div} \mathbf{v} = 0, \tag{1}$$

$$\begin{aligned} \rho \frac{d\mathbf{v}}{dt} + \nabla \left(p_\perp + \frac{B^2}{8\pi} \right) - \frac{1}{4\pi} (\mathbf{B} \cdot \nabla) \mathbf{B} = \\ = \rho \mathbf{g} + \left(p_\perp - p_\parallel \right) \left[\mathbf{h}_B \operatorname{div} \mathbf{h}_B + (\mathbf{h}_B \cdot \nabla) \mathbf{h}_B \right] + \\ + \mathbf{h}_B \left(\mathbf{h}_B \cdot \nabla \right) \left(p_\perp - p_\parallel \right), \end{aligned} \tag{2}$$

$$\frac{d}{dt} \frac{p_\parallel B^2}{\rho^3} = -\frac{B^2}{\rho^3} \left[B \left(\mathbf{h}_B \cdot \nabla \right) \left(\frac{S_\parallel}{B} \right) + \frac{2 S_\perp}{B} \left(\mathbf{h}_B \cdot \nabla \right) B \right], \tag{3}$$

$$\frac{d}{dt}\frac{p_\perp}{\rho B} = -\frac{B}{\rho}\left(\mathbf{h}_B\cdot\nabla\right)\left(\frac{S_\perp}{B^2}\right), \tag{4}$$

$$\frac{d}{dt}\frac{S_\parallel B^3}{\rho^4} = -\frac{3p_\parallel B^3}{\rho^4}\left(\mathbf{h}_B\cdot\nabla\right)\left(\frac{p_\parallel}{\rho}\right), \tag{5}$$

$$\frac{d}{dt}\frac{S_\perp}{\rho^2} = -\frac{p_\parallel}{\rho^2}\left[\left(\mathbf{h}_B\cdot\nabla\right)\left(\frac{p_\perp}{\rho}\right) + \frac{p_\perp}{\rho}\frac{p_\perp - p_\parallel}{p_\parallel B}\left(\mathbf{h}_B\cdot\nabla\right)B\right], \tag{6}$$

$$\frac{d\mathbf{B}}{dt} + \mathbf{B}\,\mathrm{div}\,\mathbf{v} - (\mathbf{B}\cdot\nabla)\mathbf{v} = 0, \tag{7}$$

$$\mathrm{div}\,\mathbf{B} = 0, \tag{8}$$

where ρ denotes the density, $p_\parallel$ and $p_\perp$ the parallel and perpendicular gas pressure, $\mathbf{B}$ the magnetic field, $\mathbf{v}$ the bulk velocity of the plasma, $\mathbf{g}$ the gravitational acceleration, $\mathbf{h}_B = \mathbf{B}/B$ is a unit vector of magnetic field, and $d/dt = \partial/\partial t + (\mathbf{v}\cdot\nabla)$ denotes the convective derivative. Here $S_\parallel$ and $S_\perp$ are the heat fluxes along the magnetic field due to parallel and perpendicular thermal kinetic motions of ions, respectively. If the heat fluxes are neglected, i.e., when $S_\parallel = 0$ and $S_\perp = 0$, we obtain with Eqs. (1)-(4), (7) and (8) a closed system of equations that is called the CGL (Chew-Goldberger-Low) equations, see the pioneering work by Chew et al. [4]. Given the 16 -moments set of Eqs. (1)-(8), one can consider including the heat fluxes to obtained a more complete form compared to the CGL equations.

In our calculations, Eqs. (1)-(6) are simplified versions of 16-moment equations, including both the ionic and electronic components of the plasma (Ramos 2003) [50]. Since the plasma is collisionless, electron and ion fluids are weakly coupled. In conditions $m_e/m_i \ll 1$, the hydrodynamic behavior of the plasma is essentially determined by the ionic component. Equations (1)-(6), as in the case of the CGL MHD model, describe the dynamics of the ion plasma, while the role of electrons is reduced only to the implementation of the plasma quasi-neutrality condition.

We consider plane-parallel geometry of the **z**-directed MHD plasma flow with shearing in **x**-direction, i.e. the equilibrium velocity $\mathbf{v}_0$ has a component only in the **z**-direction, which varies on the **x**-axis, $\mathbf{v}_0 = (0, 0,\ \mathrm{V}_0(x))$. Let the background magnetic field $\mathbf{B}_0 = const$ is directed along the **z**-axis. We assume also that the background state with non-zero heat fluxes is homogeneous (the gravitational acceleration, $g = 0$, and the quantities $\rho_0, p_{\perp 0}, p_{\parallel 0}, B_0, S_{\perp 0}, S_{\parallel 0}$ are constant).

We consider the stability of the such system with respect to linear perturbations of all the physical variables, according to the form $f = f_0 + f'(x, y, z, t)$, where the perturbation $f'(x, y, z, t) \sim F(x)\exp\left[i\left(k_y y + k_z z - \omega t\right)\right]$. So we Fourier

decompose the perturbation with respect to y, z, and t, as all the coefficients in the differential equations are only depending on x. Here, ω is the wave frequency and k_y, k_z are the wave numbers which means that the wave vector $\mathbf{k}$ lies in the (y, z) plane. After linearization of the set of Eqs. (1)-(8), we obtain

$$\frac{\rho'}{\rho_0} = \frac{k_y}{\omega_z}\mathrm{v}_y + \frac{k_z}{\omega_z}\mathrm{v}_z - \frac{i}{\omega_z}\frac{\partial \mathrm{v}_x}{\partial x}, \tag{9}$$

$$\rho_0\omega_z\mathrm{v}_x + i\frac{\partial p'_\perp}{\partial x} + i\frac{B_0}{4\pi}\frac{\partial B_z}{\partial x} + \frac{B_0}{4\pi}k_z B_x - p_\Delta k_z\frac{B_x}{B_0} = 0, \tag{10}$$

$$\rho_0\omega_z\mathrm{v}_y - k_y\left(p'_\perp + \frac{B_0}{4\pi}B_z\right) + \frac{B_0}{4\pi}k_z B_y - p_\Delta k_z\frac{B_y}{B_0} = 0, \tag{11}$$

$$\rho_0\omega_z\mathrm{v}_z + i\rho_0 V_0'(x)\mathrm{v}_x + i\frac{p_\Delta}{B_0}\frac{\partial B_x}{\partial x} - \frac{p_\Delta}{B_0}k_y B_y - k_z p'_\parallel = 0, \tag{12}$$

$$p'_\perp = \frac{k_z}{\omega_z}\left(S'_\perp - 2S_{\perp_0}\frac{B'}{B_0}\right) + p_{\perp_0}\left(\frac{B'}{B_0} - \frac{\rho'}{\rho_0}\right), \tag{13}$$

$$p'_\parallel = \frac{k_z}{\omega_z}\left(S'_\parallel - S_{\parallel_0}\frac{B'}{B_0} + 2S_{\perp_0}\frac{B'}{B_0}\right) - p_{\parallel_0}\left(2\frac{B'}{B_0} + 3\frac{\rho'}{\rho_0}\right), \tag{14}$$

$$S'_\perp = \frac{p_{\parallel_0}p_{\perp_0}k_z}{\rho_0\omega_z}\left(\frac{p'_\perp}{p_{\perp_0}} - \frac{\rho'}{\rho_0} + \frac{p_\Delta B'}{p_{\parallel_0}B_0}\right) + 2S_{\perp_0}\frac{\rho'}{\rho_0}, \tag{15}$$

$$S'_\parallel = 3\frac{p^2_{\parallel_0}k_z}{\rho_0\omega_z}\left(\frac{p'_\parallel}{p_{\parallel_0}} - \frac{\rho'}{\rho_0}\right) - S_{\parallel_0}\left(3\frac{B'}{B_0} - 4\frac{\rho'}{\rho_0}\right), \tag{16}$$

$$\omega_z B_x + B_0 k_z \mathrm{v}_x = 0, \tag{17}$$

$$\omega_z B_y + B_0 k_z \mathrm{v}_y = 0, \tag{18}$$

$$\frac{\partial B_x}{\partial x} + ik_y B_y + ik_z B_z = 0. \tag{19}$$

Inserting (15) and (16) into (13) and (14), we can write

$$p'_\perp = p_{\perp_0}\frac{a_1(x)}{a_0(x)}\frac{B_z}{B_0} + p_{\perp_0}\frac{a_2(x)}{a_0(x)}\frac{\rho'}{\rho_0}, \tag{20}$$

$$p'_\parallel = p_{\parallel_0}\frac{b_1(x)}{b_0(x)}\frac{B_z}{B_0} + p_{\parallel_0}\frac{b_2(x)}{b_0(x)}\frac{\rho'}{\rho_0}. \tag{21}$$

Here $p_\Delta = p_{\parallel 0} - p_{\perp 0}, V_0'(x) = \partial \mathrm{V}_0/\partial x$, and $\omega_z = \omega - k_z V_0(x)$ is the Doppler shifted frequency. We can reduce the system of Eqs. (9)-(19) to one

single second-order differential equation by using the obvious relations between the physical variables

$$\mathrm{v}_x = -\frac{\omega_z}{B_0 k_z} B_x, \tag{22}$$

$$\mathrm{v}_y = -\frac{\omega_z}{B_0 k_z} \frac{i k_y A}{\beta_A} \frac{\partial B_x}{\partial x}, \tag{23}$$

$$\mathrm{v}_z = -\frac{\omega_z}{B_0} \frac{i A \beta_1}{\beta_\star} \frac{\partial B_x}{\partial x}, \tag{24}$$

$$B_y = \frac{i k_y A}{\beta_A} \frac{\partial B_x}{\partial x}, \tag{25}$$

$$B_z = \frac{i k_z A}{\beta_\star} \frac{\partial B_x}{\partial x}, \tag{26}$$

$$\rho' = \frac{\rho_0}{B_0} \frac{i k_z A \left(1-\beta_1\right)}{\beta_\star} \frac{\partial B_x}{\partial x}, \tag{27}$$

$$p'_\perp = \frac{a_1 + \left(1-\beta_1\right) a_2}{a_0} \frac{p_{\perp 0}}{B_0} \frac{i k_z A}{\beta_\star} \frac{\partial B_x}{\partial x}, \tag{28}$$

$$p'_\parallel = \frac{b_1 + \left(1-\beta_1\right) b_2}{b_0} \frac{p_{\parallel 0}}{B_0} \frac{i k_z A}{\beta_\star} \frac{\partial B_x}{\partial x}. \tag{29}$$

Substituting all these relationships and thus eliminating variables, we obtain

$$\frac{\partial}{\partial x}\left(A(x) \frac{\partial B_x}{\partial x}\right) - \beta_A(x) B_x = 0, \tag{30}$$

where

$$A(x) = \frac{\beta_A \beta_\star}{k_y^2 \beta_\star + k_z^2 \beta_A}, \tag{31}$$

and

$$\begin{aligned} &\beta_A = \beta - \bar{\alpha} - \frac{1}{\eta^2}, \quad \beta_\star = \beta_0 - \alpha \frac{a_2}{a_0} \beta_1, \\ &\beta_0 = \alpha \frac{a_1 + a_2}{a_0} + \beta, \quad \beta_1 = \frac{b_0 \bar{\alpha} - b_1 - b_2}{b_0/\eta^2 - b_2}, \end{aligned} \tag{32}$$

while the coefficients $a_{0,1,2}$ and $b_{0,1,2}$ are determined as

$$\begin{aligned} &a_0 = 1 - \eta^2, \quad b_0 = 1 - 3\eta^2, \\ &a_1 = 1 - 2\gamma\eta - \bar{\alpha}\eta^2, \quad b_1 = 2\gamma\eta(\alpha - 2) - 2, \\ &a_2 = 1 + 2\gamma\eta - \eta^2, \quad b_2 = 3 + 4\gamma\eta - 3\eta^2. \end{aligned} \tag{33}$$

In the above equations, the following dimensionless parameters were used for the basic unperturbed physical quantities and the indexes zero are dropped for simplification of the notation:

$$\begin{aligned} &\alpha = \frac{p_\perp}{p_\parallel}, \quad \bar{\alpha} = 1 - \alpha, \quad \beta = \frac{B^2}{4\pi p_\parallel} = \frac{\mathrm{v}_\mathrm{A}^2}{c_\parallel^2}, \quad c_\parallel^2 = \frac{p_\parallel}{\rho}, \\ &\eta = \frac{c_\parallel k_z}{\omega_z}, \quad \gamma_\parallel = \frac{S_\parallel}{p_\parallel c_\parallel}, \quad \gamma_\perp = \frac{S_\perp}{p_\perp c_\parallel}, \quad \gamma = \gamma_\parallel = \gamma_\perp. \end{aligned} \tag{34}$$

The case where $\gamma = \gamma_\parallel = \gamma_\perp$ is a simplified approach. Here, $c_\parallel$ denotes parallel sound speed, v_A is the Alfvén velocity, α the anisotropy parameter, γ the background heat fluxes parameter, and β is inversely proportional to the plasma beta ($\beta = 2/\beta_{pl}$). We also denote θ for the wave propagation angle relative to the magnetic field, i.e., $k_z = k\cos\theta$, $k_y = k\sin\theta$, and after denoting $\cos^2\theta \equiv \ell$, we can write $k_z = k\sqrt{\ell}$ and $k_y = k\sqrt{1-\ell}$, and let $k > 0$.

3. EIGEN OSCILLATIONS OF THE LAYER WITH SHEARING FLOW

The coefficients of obtained second order ordinary differential wave equation Eqs.(30) are variable, and they are complex functions of $V_0(x)$. Furthermore, the velocity profile $V_0(x)$ is still an arbitrary function of the x-coordinate. In the case when two plasma flows adjoin, there arises a transition layer with a finite thickness between them. The thickness of the transition layer is determined by the flow velocities and physical parameters in each flow. In the simplest case, to mimic this situation we consider an analytical velocity profile given by the hyperbolic function of

$$V_0(x) = \frac{V_{02}e^{\sigma x} + V_{01}e^{-\sigma x}}{e^{\sigma x} + e^{-\sigma x}}, \quad \sigma \geqslant 0. \tag{35}$$

Here $V_0(-\infty) = V_{01}$ and $V_0(+\infty) = V_{02}$ are the limit velocities and let $h = V_{01}/V_{02} \geqslant 1$, $V_0(0) = (V_{01} + V_{02})/2 = \bar{V}_0$ is the average of the two velocities. In the Eqs.(35) the σ parameter characterizes the thicknesses of the transition layer L. Figure 1 shows schematically the various profiles of $V_0(x)$ for different values of σ. As the parameter $\sigma L > 0$ increases, the width of the transition layer between the two flows sharply decreases and becomes a discontinuity ($\sigma L \gg 1$) between the velocities V_{01} and V_{02}. For the small $\sigma L \ll 1$ the width of the transition layer becomes very large.

Let's introduce the next notations

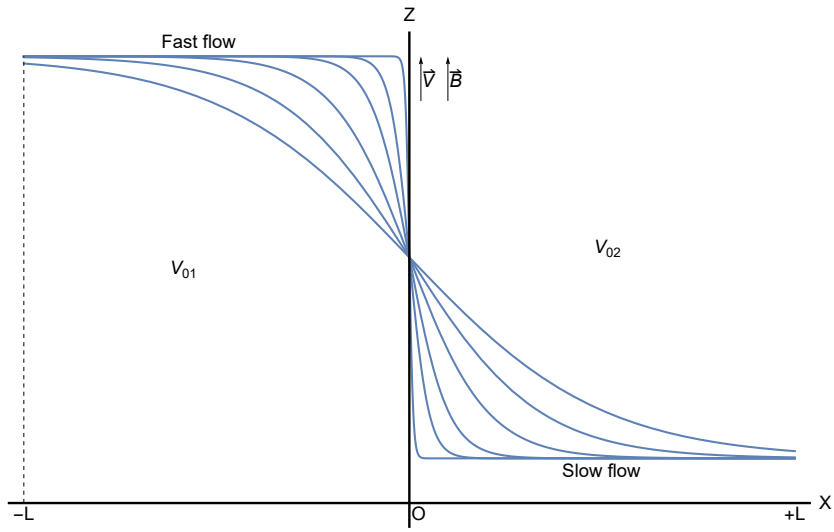

Fig. 1. Schematic representation of MHD plasma shearing flow. Different line profiles correspond to different values of $\sigma_L = \sigma L$ in (35).

$$y(x) = \frac{B_x}{B_0},\ \xi(x) = \frac{\omega - k_z V_0(x)}{c_\parallel k_z},\ \beta_A(x) = \alpha + \beta - 1 - \xi^2,$$
$$\beta_*(x) = \beta + 2\alpha + 2\alpha^2 \cdot \frac{\xi^4 + 2\gamma\xi^3 + 2\gamma^2\xi^2 - 5\xi^2 - 6\gamma\xi + 3}{(\xi^2 - 1)\,(\xi^4 - 6\xi^2 - 4\gamma\xi + 3)}. \tag{36}$$

Then we can write the Eqs.(30) as

$$\frac{d}{dx}\left(\frac{\beta_A\beta_*}{k_y^2\beta_* + k_z^2\beta_A}\frac{dy(x)}{dx}\right) - \beta_A y(x) = 0. \tag{37}$$

As noted in the Introduction, we will be interested in the excitation of waves and instabilities due to the free energy of a flow with a gradient. As we showed earlier in (Ismailli et al.2018) [32], waves can grow due to the energy of the flow if these waves are in resonance with the flow, i.e. when the phase velocity along the flow is close to the average flow speed, $\omega \sim k_z\bar{V}_0$. Therefore, let $\omega = k_z\bar{V}_0(1 + \Omega)$, where Ω is the spectral parameter to be determined. Then $\xi(x) = M[\Omega + \Delta\tanh(\sigma x)]$, where $M = \bar{V}_0/c_\parallel$ is the Mach number, $\Delta = (h-1)/(h+1)$ is the shear rate. Note that $0 \le \Delta \le 1$ and hence, $\Delta = 0$ corresponds to a uniform flow ($V_{01} = V_{02}$) and $\Delta = 1$, if the plasma slips over a more static environment ($V_{02} = 0$).

Now let's move on to the dimensionless independent variable $\tau = x/L$ in Eq.(37). Designating $\sigma_L = \sigma L$, $\bar{k} = kL$ and so $\xi(\tau) = M[\Omega + \Delta\tanh(\sigma_L\tau)]$ we have

$$\left(\mathcal{P}y'\right)' - Qy = 0, \tag{38}$$

where $y' = y'(\tau)$ and

$$\mathcal{P}(\tau) = \frac{\beta_A \beta_*}{(1-l)\beta_* + l\beta_A}, \quad Q(\tau) = \bar{k}^2 \beta_A. \tag{39}$$

Our main goal in the next step is solving the boundary value problem based on the Eq. (38), to find the complex spectral parameter Ω with $\Omega_i = \mathrm{Im}(\Omega) \neq 0$. For such a problem, we can use the fact that in the real integration axis τ for the coefficients (39) it is possible to satisfy the conditions $\mathcal{P}(\tau) \neq 0$ and $Q(\tau) \neq 0$.This situation makes it possible to find WKB (Wentzel-Kramers-Brillouin) approximate analytical solutions of the second-order equation (38). So, for the complex $\mathcal{P}(\tau), Q(\tau) \Rightarrow C^2(I)$ functions assuming $\mathrm{Re}(QP) \geq 0$ we can write the leading expansion term of WKB solutions, e.g. in (Fedoryuk M.1983) [19] as

$$\tilde{y}_{1,2} = \frac{e^{\pm iS(\tau)}}{\sqrt{w}}, \quad w = \sqrt{\mathcal{P}Q}, \quad S = \int_{\tau_0}^{\tau} \sqrt{-\frac{Q}{\mathcal{P}}} d\tau. \tag{40}$$

The deviation of exact solutions $y_{1,2}$ from WKB ones $\tilde{y}_{1,2}$ is determined by the right-hand side of the following expression

$$\left| \frac{y_{1,2}}{\tilde{y}_{1,2}} - 1 \right| \leq T_{WKB} = 2\left(e^{2\mu_I(\tau)} - 1 \right) < 1, \tag{41}$$

where

$$\mu_I(\tau) = \left| \int_{\tau_0}^{\tau} |\mu| d\tau \right|, \quad \mu(\tau) = \frac{1}{8w^5} \left[\left(\mathcal{P}w' \right)' w - \frac{5}{4} \mathcal{P} \left(w' \right)^2 \right]. \tag{42}$$

Two independent solutions of the Eqs. (38) with accurasy of (41) can be represented in the form

$$y(\tau) = \frac{1}{\sqrt{w}} \left(C_1 e^{iS} + C_2 e^{-iS} \right), \tag{43}$$

where $C_{1,2} = \mathrm{const}$ to be determined from the boundary conditions. Let's limit the region of integration along the x axis within $-L \leq x \leq +L$. This means that the shearing layer is located in this area (see in the Fig.1). Let's limit the layer on the left $\tau = -1$ and right side $\tau = +1$ with hard boundaries, which corresponds to natural conditions of $y(\pm 1) = 0$.

Let $\tau_0 = 0$, $u(\tau) = \sqrt{-Q/\mathcal{P}}$ and

$$S_+ = \int_0^1 u d\tau, \quad S_- = \int_{-1}^0 u d\tau, \quad I = S_- + S_+ = \int_{-1}^1 u d\tau. \tag{44}$$

From the boundary conditions of $y(\pm 1) = 0$ we get that $\exp(2iS_-) = \exp(-2iS_+)$ or

$$\sin(I) = 0; \quad I = n\pi, n = 0, \pm 1, \pm 2, \cdots \tag{45}$$

This is the desired dispersion equation for the eigen oscillations of an anisotropic plasma layer with shear flow. Introducing the notation $z = \tanh(\sigma_L \tau)$, $\xi_\pm = M(\Omega \pm \Delta z)$ and $b = \tanh(\sigma_L)$ let us present this equation in the form

$$\int_0^1 \left(\sqrt{f(\xi_+)} + \sqrt{f(\xi_-)} \right) d\tau = \lambda_n, \tag{46}$$

or

$$\int_0^b \frac{\sqrt{f(\xi_+)} + \sqrt{f(\xi_-)}}{1 - z^2} dz = \sigma_L \lambda_n, \tag{47}$$

where

$$f(\xi) = -\frac{(1-l)\beta_*(\xi) + l\beta_A(\xi)}{\beta_*(\xi)}, \quad \lambda_n = \frac{n\pi}{kL}, = \frac{\lambda_\perp n}{2L}. \tag{48}$$

The λ_n parameter is the ratio of the wavelength $\lambda_\perp$ in the (y-z) plane ($k^2 = k_y^2 + k_z^2$ and $k = 2\pi/\lambda_\perp$) to the geometric width ($2L$) of the plasma layer with a flow that is a multiple of the number of unevenly located nodes n of the eigenfunctions along the x axis. If we denote the scale of fluctuation structures caused by shear flow along the x-axis as $\lambda_x = 2L/n$, then $\lambda_n = \lambda_\perp/\lambda_x$.

The eigenfunctions taking into account (44) and (45) can be represented in the form

$$y(\tau) = (-1)^{n+1} \frac{C}{w} \sin\left(\int_{-1}^0 u(\tau) d\tau - \int_\tau^0 u(\tau) d\tau \right), \quad -1 \le \tau \le 0 \tag{49}$$

$$y(\tau) = \frac{C}{w} \sin\left(\int_0^1 u(\tau) d\tau - \int_0^\tau u(\tau) d\tau \right), \quad 0 \le \tau \le 1 \tag{50}$$

where $C = \text{const}$.

4. INSTABILITIES IN HOMOGENEOUS FLOW

Let us briefly consider the well-known fire-hose and mirror instabilities of an anisotropic plasma (in the domains of $\alpha < 1$ and $\alpha > 1$, correspondingly) with a uniform flow, so that we can compare them with modified instabilities due to shearing of the flow. For a homogeneous flow $\Delta = 0$, and therefore $\xi_+ = \xi_- = M\Omega = \Omega_*$, $f(\xi_+) = f(\xi_-) = f(\Omega_*)$. Then dispersion equation (47) reduces to $f(\Omega_*) - \bar{\lambda}_n^2 = 0$, where $\bar{\lambda}_n = \lambda_n/2$. This is an 8th order polynomial on the spectral parameter Ω_*:

$$c_8\Omega_*^8 + c_7\Omega_*^7 + c_6\Omega_*^6 + c_5\Omega_*^5 + c_4\Omega_*^4 + c_3\Omega_*^3 + c_2\Omega_*^2 + c_1\Omega_* + c_0 = 0. \tag{51}$$

Here

$$
\begin{aligned}
c_0 &= 6(\bar{\lambda}_n^2 - l + 1)\alpha^2 - 6(\bar{\lambda}_n^2 - l/2 + 1)\alpha - 3(\beta\bar{\lambda}_n^2 - l + \beta),\\
c_1 &= -12\gamma(\bar{\lambda}_n^2 - l + 1)\alpha^2 + 8\gamma(\bar{\lambda}_n^2 - l/2 + 1)\alpha + 4\gamma(\beta\bar{\lambda}_n^2 + \beta - l),\\
c_2 &= 2(\bar{\lambda}_n^2 - l + 1)(2\gamma^2 - 5)\alpha^2 + 18(\bar{\lambda}_n^2 - l/2 + 1)\alpha + 9(\beta\bar{\lambda}_n^2 - 2l/3 + \beta),\\
c_3 &= 4\gamma[(\bar{\lambda}_n^2 - l + 1)\alpha^2 - 2(\bar{\lambda}_n^2 - l/2 + 1)\alpha - \beta(\bar{\lambda}_n^2 + 1)],\\
c_4 &= 2(\bar{\lambda}_n^2 - l + 1)\alpha^2 - 14(\bar{\lambda}_n^2 - l/2 + 1)\alpha - 7(\beta\bar{\lambda}_n^2 + 2l/7 + \beta),\\
c_5 &= 4\gamma l, \quad c_6 = (2\bar{\lambda}_n^2 - l + 2)\alpha + \beta\bar{\lambda}_n^2 + 6l + \beta, \quad c_7 = 0, \quad c_8 = -l.
\end{aligned}
$$

Note that this dispersion equation for an infinite medium $L = \infty$, therefore $\bar{\lambda}_n = 0$, was studied in detail in (Dzhalilov and Kuznetsov,2013) [12] and the obtained results were compared with the results of low-frequency kinetics. The good agreement between the thresholds and growth rates of low-frequency instabilities obtained in the kinetic and MHD approaches indicates that the MHD model based on the 16-moment fluid equations is quite applicable for the hydrodynamic description of collisionless plasma.

Here first of all we want to show how the spatial limitation of the plasma layer ($-\infty < L < +\infty$) along the x-axis can influence to the known instabilities growing. Note that in this case the classical incompressible fire-hose modes are separated (see in the Eq. (30): the term $\beta_A = 0$ describes the frequency of Alfvén oscillations). Other modes are described by the Eq. (51), coefficients of which depend on the parameters α, β, γ, l and λ_n. We will simplify the problem, eliminating the influence of heat flux, $\gamma = 0$ and fix the magnetic parameter, let $\beta = 0.1$ (weak magnetic field). For an infinite layer width, $\lambda_n = 0$, the dependence of the instability growing rates of aperiodic in the moving fluid frame modes ($\Omega_r = \mathrm{Re}(\Omega) = 0$) - oblique fire hose and mirror instabilities on the wave propagation angle l and on the anisotropy parameter of α is shown in Fig. 2. These parameter dependence growing rate results are well known.

To clarify the role of flow layer width limitation, let us take two typical cases from the figure 2: $\alpha = 0.5$ for the fire-hose mode and $\alpha = 1.4$ for mirror modes. As it follows from Figure 3, with increasing parameter λ_n, the region of existence of fire-hose modes sharply narrows and it disappears if $\lambda_n > 1$. The opposite situation arises for mirror modes: with increasing parameter λ_n, the region of occurrence of mirror instability on parameter l expands and covers all possible propagation angles, $0 \le l \le 1$. With increasing λ_n, the growth rate of mirror modes increases to the maximum asymptotic value (in the case under consideration, $(M\Omega_i)_{max} = 0.53$), i.e. the instability of mirror modes becomes stronger than fire-hose modes.

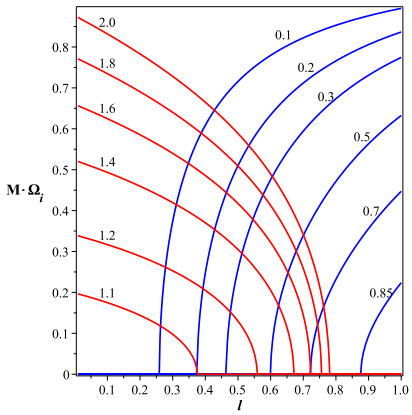

Fig. 2. Dependence of the growing rates of quasi-parallel fire hose (blue lines) and quasi-perpendicular mirror (red lines) instabiliies from $l = \cos^2(\theta)$ in different α (numbers at curves) for $\bar{\lambda}_n = 0$. With decreasing of anisotropy $\alpha \to 1$ both instabilities fade out

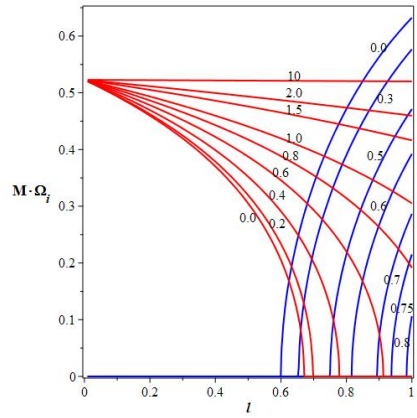

Fig. 3. Dependence of the growing rates of fire hose (blue lines) and mirror (red lines) instabiliies from $l = \cos^2(\theta)$ in different $\bar{\lambda}_n \neq 0$ (numbers at curves). For the mirror modes $\alpha = 1.4$ and fire-hose modes $\alpha = 0.5$ are chosen as the typical examples.

5. OBLIQUE FIRE-HOSE MODE INSTABILITY IN SHEARING FLOW

Now let us consider how the instabilities change when the flow is sheared. In this case, two additional parameters, Δ and σ_L, are added to the problem for which the rather difficult integral dispersion Eq. (47) must be solved. In this work we will restrict ourselves to oblique fire-hose modes only. We fix the plasma anisotropy parameter $\alpha = 0.5$, the magnetic parameter $\beta = 0.1$, the propagation angle parameter $l = 0.9$, heat flux parameter $\gamma = 0$ and the Mach number $M = 5$ (supersonic flow). The dependence of the fire-hose instability growing rate on Δ for various values of λ_n and σ_L is shown in figures 4 and 5.

It is characteristic that with the appearance of the slightest shifting in velocity, the instability intensifies sharply and reaches a maximum. For the small λ_n a minor shift is sufficient to enhance the instability. A similar picture is obtained when changing the σ_L parameter. At small scales of the velocity gradient ($\sigma_L \to 0$), the flow is almost uniform and the instability is weak. As the gradient increases, instability sharply increases.

In the figures 6 and 7 we show the results of the dependence of instability growth rate of fire-hose modes Ω_i on the parameter λ_n for the different given Δ and σ_L parameters values. These examples cover both a very wide plasma layer ($kL \gg 1$) and a narrow layer ($kL \ll 1$). We see that the hose modes that arise in a wide layer as body waves disappear as the layer width decreases and goes to

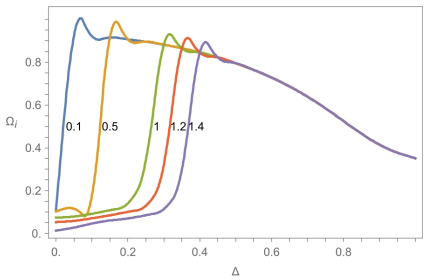

Fig. 4. The dependence of instability growing rate Ω_i of fire-hose modes on the shearing rate of plasma supersonic flows Δ at different values of λ_n (numbers at curves) when $\sigma_L = 1$.

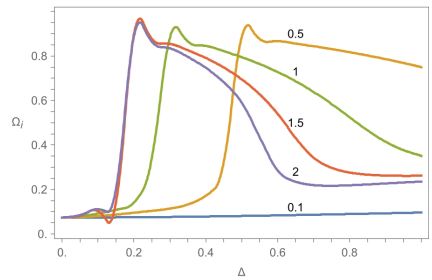

Fig. 5. The dependence of instability growing rate Ω_i of fire-hose modes on the shearing rate of plasma supersonic flows Δ at different values of σ_L (numbers at curves) when $\lambda_n = 1$.

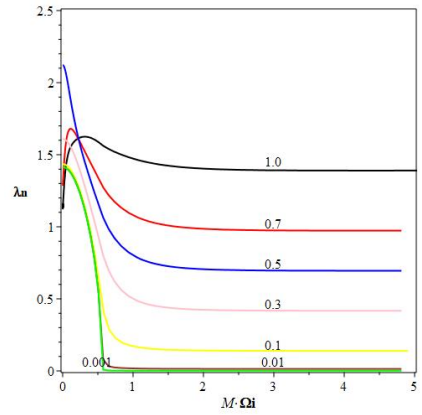

Fig. 6. The dependence $\lambda_n = n\pi/kL$ from the instability growing rate $M\Omega_i$ of fire-hose modes at the different values of the shearing rate of $M\Delta$ (numbers at curves) for the case of $\sigma_L = 3$ and $\gamma = 0$.

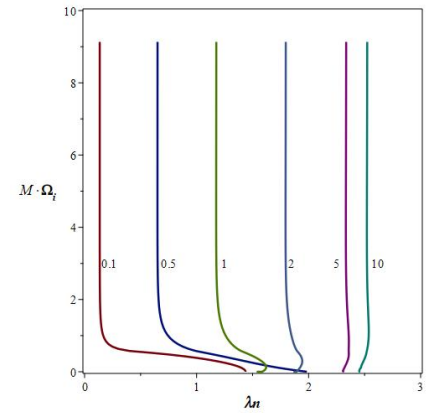

Fig. 7. The dependence of instability growing rate $M\Omega_i$ of fire hose modes on the λ_n at different values of σ_L (numbers at the curves) when $M\Delta = 1.5$

zero. Note that the discontinuous case corresponds to $L \to 0$ and $\sigma_L \gg 1$.

5.1. On the validity of the WKB solutions

In this work, we solved the boundary value problem based on the WKB solutions (40). Taking into account that the coefficients of the equation (37) are the ratio of polynomials, and the eigenfunctions are expressed by complex irrational expressions, it is important to show the smoothness of the eigenfunctions and the domain of definition of the obtained results. In this issue, the main is that the

sought and found eigenvalues (oscillation frequencies) are complex, and are found such values at which the divergence of terms in the WKB expansion is excluded. Proof of this is Figure 8, where for the found eigenvalues (for four cases), the dependence of the T_{WKB} deviation of the WKB solutions from the exact one (41) is calculated as a function of $n = 0, 1, 2, \cdots$ numbers. As can be seen, the curves are smooth, and the region of validity $T_{WKB} < 1$ of the illustrated results is located in the region of larger n. These cases in the Fig.8 are:

1) $\gamma = 0, \sigma_L = 3, \Omega_r = 0, M\Omega_i = 1.0604, \lambda_n = 2.1203$;
2) $\gamma = 0, \sigma_L = 3, M[\Omega_r, \Omega_i] = [0.9007, 0.1], \lambda_n = 2.7724$;
3) $\gamma = 0.7, \sigma_L = 3, M[\Omega_r, \Omega_i] = [0.5, 0.3419], \lambda_n = 2.2291$;
4) $\gamma = 0.7, \sigma_L = 0.55, M[\Omega_r, \Omega_i] = [0.10201, 0.3248], \lambda_n = 1.4473$.

These eigenvalues have been found in the parameter values of: $M = 5, \Delta = 0.3, \alpha = 0.5, \beta = 0.1$ and $l = 0.9$.

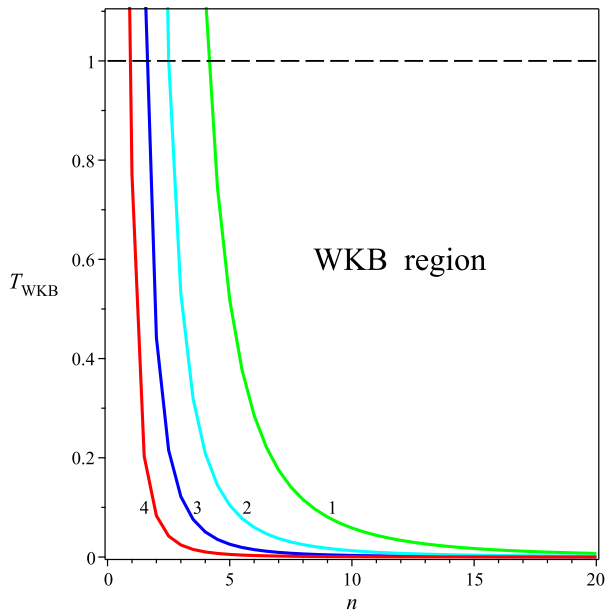

Fig. 8. The range of applicability of the obtained results based on the WKB solutions, $T_{WKB} < 1$, for four cases of eigenvalues (see the text).

6. CONCLUSIONS

In this work, we considered a layer of anisotropic collisionless plasma with a finite width. It was assumed that a homogeneous plasma flows along the magnetic field has a transverse velocity gradient. The stability of the plasma layer

to small disturbances in the MHD description was studied on the basis of moment equations obtained from the Vlasov kinetic equation taking into account the heat flux along the flow. A wave equation is derived, which is a second-order ordinary differential equation with complex variable coefficients. To solve the boundary value problem and find the complex spectral parameter that determines the growth rate of instability, the WKB approximation was used to find asymptotic solutions for the case of a hyperbolic velocity profile. A general integral dispersion equation, based on these solutions is obtained. This equation describes all types of instabilities in the presence of heat flux along the magnetic field, well studied for infinite stationary anisotropic plasma (Dzhalilov,Kuznetsov ,2008,2011,2013;Dzhalilov,Ismailli 2023). [12–15] These instabilities, such as parallel and oblique firehose modes, mirror modes, KHI modes, and others in an infinite medium and velocity discontinuities, arise under certain conditions determined by the plasma parameters.

Note that the case considered here, the spatially limited plasma layer with a transverse gradient in flow velocity, is a more realistic case that occurs in various cosmic situations. Therefore, studying the effect of plasma confinement on known properties of instabilities, modification of them, and the interaction of various modes due to a shearing of flow velocity in the presence of a heat flux are poorly studied problems. The resulting general dispersion equations allow us to move to known limiting cases - into an infinite medium without a shearing in velocity and an extremely narrow layer with a jump in the velocity (discontinuity limit). The first important result is that the spatial limitation of the plasma greatly affects the instabilities of the mirror and oblique fire-hose mode instabilities. Namely, reducing the layer width greatly enhances the mirror instability, and strongly suppresses the hose instability. Further, we limited ourselves here to study how the spatial gradient of the plasma flow, characterized by two σ_L and Δ parameters, affects to the properties of oblique hose instability in a limited layer. It was found that the spatial gradient in flow velocity greatly enhances this instability. With a narrowing of the layer width ($L \to 0$) and an increase of the velocity gradient ($\sigma_L \gg 1$), the body hose modes transform into surface KH modes existing on the discontinuity surface between the two parts of flow. Note that the results presented here are only for aperiodic modes ($Re(\Omega) = 0$) without taking into account the influence of heat flux. For the same fixed anisotropic plasma and magnetic parameters (α and β) and propagation angle relative to the magnetic field (l), in addition to aperiodic instabilities, periodic instabilities also arise ($Re(\Omega) \neq 0$, $Im(\Omega) \neq 0$), as a result of interaction with other modes (most likely with KH modes, see (Dzhalilov,Ismailli ,2023) [15]. These results are not included here.

In future works, the mirror and other shear instabilities will be considered. It is especially interesting how the KHI is modified as a results of interaction with

other modes, and what happens during the transition from a jump in velocity (discontinuity) to a plasma layer with a finite width and with a transverse gradient. In conclusion, we note that the facts of increase of hose instability due to the velocity shearing are important for the general theory of turbulence generation in anisotropic space plasmas.

ACKNOWLEDGMENTS

We would like to extend our special thanks to Jamila Tagiyeva, Head of the Scientific Results Processing and Publishing Sector at N.Tusi Shamakhy Astrophysical Observatory, for her invaluable editing of this article.

REFERENCES

1. Bruno R., Carbone V., 2013, Liv. Rev. Sol. Phys., **10**, 2.

2. Bale S. D., Kasper J. C., Howes G. G., Quataert E., Salem C., Sundkvist D., 2009 Phys. Rev. Lett. **103**, 211101.

3. Blasl,K. A., Nakamura, T. K. M., Plaschke, F., et al. 2022, Plasma Physics Reports, **29**, 012105.

4. Chew G. F., Goldberger M. L., Low F. E., Proc. R. Soc., 1956 London, A **236**, 112.

5. Chac'on L., Knoll D. A., Finn J. M., 2003, Phys. Lett. A **308**, 187.

6. Chandrasekhar, S. 1961, Hydrodynamic and Hydromagnetic Stability (Oxford University Press).

7. Choudhury S. R., Patel V. L., 1985, Phys. Fluids,**28**, 3292.

8. Choudhury S. R., 1986, J. Plasma Phys.,**35**, 375.

9. Cranmer S. R., Asgari-Targhi M., Miralles M. P., et al., 2015, RSPTA(Royal Society of London Philosophical Transactions Series A), **373**, 20140148.

10. Chasapis A., Matthaeus W. H., Parashar T. N., et al., 2017, ApJ, **836**, 247.

11. Delamere M. X., Nykyri P., Otto K., Eriksson A., Chai S., L., et al., 2024, Journal of Geophysical Research; Space, **129**,e2023JA032234.

12. Dzhalilov N. S., V. D. Kuznetsov, 2013, Plasma Physics Reports, **39**, 12, 1007.

13. Dzhalilov N. S., Kuznetsov V. D., Staude J., 2008, A&A , **489**, 769.

14. Dzhalilov N. S., Kuznetsov V. D., Staude J., 2011, Contributions to Plasma Physics, **51**, 621.

15. Dzhalilov N.S., Ismailli R., 2023, MNRAS **520**, 1526.

16. Foullon C., Verwichtel E., Nakariakov V. M., Nykyri K., Farrugia C. J., 2011, ApJ, **729**, L8.

17. Faganello M., Califano F., Pegoraro F., 2008, Physical Review Letters, **100**,015001.

18. Faganello M., Califano F., 2017, Journal of Plasma Physics, **83**, 535830601.

19. Fedoryuk M. V., 1983, Asymptotic methods in the theory of ordinary linear differential equations, Moscow, Nauka, 352.

20. Gary S. P., Hughes R. S., Wang, J., 2016, ApJ, **816**, 102.

21. Guzzil G., Settino A.,Valentini F., Malara F., 2021, A&A,**645**,A147.

22. Hasegawa, A., 1975, Plasma Instabilities and Nonlinear Effects, 94, Springer- Verlag, New York.

23. Hasegawa H., Fujimoto M., Phan T.-D., et al., 2004, Nature, **430**, 755.

24. Hau L.N., B. U. O¨ . Sonnerup, Geophys. Res. Lett.,1993 **20**, 1763.

25. Hellinger P, Tr'avn'ıˇcek P, Kasper JC, Lazarus AJ (2006) Geophys Res Lett 33:L09101.

26. Hellinger P., Matsumoto H., Geophys J., Res.,2000, **105**, 10519.

27. Hollweg J. V., 1987, ApJ, **312**, 880.

28. Henri P., Cerri S. S., Califano F., et al., 2013, Physics of Plasmas, **20**,102118.

29. Hamlin N. D., Newman W. I., 2013, Phys. Rev. E, **87**, 043101.

30. Hasegawa H., Nakamura T. K. M., Gershman,D. A. J., et al., Journal of Geophysical Research 2020.

31. Hollweg J. V., Kaghashvili E. Kh., 2012, Astrophys. J., **744**, 114.

32. Ismailli R. F., Dzhalilov N. S. , Shergelashvili B. M. , Poedts S., Pirguliyev M. Sh. 2018, Physics of Plasmas **25**.

33. Jain N., Buchner J., Comishel H., Motschmann U., 2021, ApJ, **919**, 103.

34. Kiyani K. H., Osman K. T., Chapman S. C., 2015, Royal Society of London Philosophical Transactions Series A, **373**, 20140155.

35. Kaghashvili E. K., 2007, Phys. Plasmas, **14**, 044502.

36. Kivelson M. G., Chen S., 1995, in Physics of the Magnetopause (Washington, DC: AGU), Geophys. Monogr. Ser., **90**

37. Loureiro N. F., Boldyrev S., 2017, Physical Review Letters, **118**, 245101.

38. Matteini L., Hellinger P., Goldstein B. E., Landi S., Velli M., Neugebauer M., 2013, Geophys J., Res., **118**, 2771.

39. Mok Y., Einaudi G., 1985, J. Plasma Phys., **33**, 199.

40. Miura, A., 1982 Phys. Rev. Lett., **49**, 779.

41. Maiorano T., Settino A., Malara F., et al., 2020, J. Plasma Phys., **86**, 825860202.

42. Marsch E., 2006, Living Reviews in Solar Physics, **3**, 1.

43. Oraevski V. N., Konikov Y. V., Chazanov G. V., Nauka, Moscow, 1985, Transport Processes in Anisotropic Near-Earth Plasma, **173**.

44. Pucci F., Onofri M., Malara F., 2014, Astrophys. J., **796**, 43.

45. Pucci F., V'asconez C. L., Pezzi O., Servidio S., Valentini F., Matthaeus W. H., Malara F., 2016, J. Geophys. Res., **121**, 1024.

46. Pucci F., Onofri M., Malara F., 2014, ApJ, **796**, 43.

47. Pezzi O., Parashar T. N., Servidio S., et al., 2017, ApJ, **834**, 166.

48. Pritchett P. L., Coroniti F. V., 1984, Journal of Geophysical Research, **89**, 168.

49. Ray T. P., Ershkovich A. I., 1983, Mon. Not. R. Astron. Soc., **204**, 821.

50. Ramos J. J., 2003, Phys. Plasmas, **10**, 3601.

51. Sisti M., Faganello M., Califano,F., et al., 2019, Geophysical Research Letters,**46**, 11, 597.

52. Telloni Daniele, et al., 2022, ApJ, **929**, 98.

53. Uchava E. S., Tevzadze A. G., Shergelashvili B. M., Dzhalilov N. S., Poedts S., 2020, Phys. Plasmas **27**, 112901.

54. Uberoi C., 1986, Planet. Space Sci., **34**, 1223.

55. Verdini A., Grappin R., Montagud-Camps V., 2019, Solar Physics, **294**, 65.

56. Vedenov A. A., Sagdeev R. Z., 1958, Sov. Phys. Dokl., **3**, 278.

57. Vasconez C. L., Pucci F., Valentini, F., et al., 2015, ApJ, **815**, 7.

58. Verscharen D., Klein K. G., Maruca B. A., 2019, Living Reviews in Solar Physics, **16**, 5.

59. Walker A. D. M., 1981, Perspectives of Earth and Space Scientists, **29**, 1119.

60. Wang B.J., L.-N. Hau, 2003, Journal of Geophysical Research, **108**, A12, 1463.